Broatch, A.; Olmeda, P.; Margot, X.; Agizza, L. (2022). A generalized methodology for lithium-ion cells characterization and lumped electro-thermal modelling. Applied Thermal Engineering. 217:1-19. https://doi.org/10.1016/j.applthermaleng.2022.119174

A generalized methodology for lithium-ion cells characterization and lumped electro-thermal modelling

Alberto Broatch[1], Pablo Olmeda[1,2], Xandra Margot[1], Luca Agizza[1]

[1]CMT – Motores Térmicos, Universitat Politècnica de València, Camino de Vera s/n 46022, Valencia, Spain

[2] Corresponding author: pabolgon@mot.upv.es; +34 963 877 658

Abstract

This paper deals with the experimental characterization and electro-thermal modeling of lithium-ion batteries. This aspect is of considerable importance to be able to have an understanding of the phenomena of heat generation and thermal behavior of a lithium-ion battery. Electrical parameters need to be characterized to properly estimate the electrical losses inside the battery and, thus, of the total heat generation. The testing methodology employed to do this is fully described. It highlights the dependency of each parameter on state of charge, current and temperature. Thermal parameters are calculated knowing the internal characteristics and composition of the cell and using available data from literature. A first order equivalent circuit model is used to simulate the electric behavior of the cell. Extrapolation models are used to accurately estimate capacity and resistive parameters for points outside the considered test matrix. The thermal behavior of the cell is modeled using a nodal network, assigning volume, heat capacity and heat generation to the nodes. The whole methodology shown can be adapted to any other chemistry, format, or capacity; furthermore, this methodology can be applied also in case of limited test matrix points, due to the implementation of extrapolation models for electrical parameters. Finally, a case study for the fast charging of a battery module is presented, to highlight the great potential of the model, not only for on-line estimation, but also for off-line studies, being the charging operation one of the most critical from the thermal management point of view.

Keywords: *lithium-ion; batteries; experimental characterization; electro-thermal modelling; fast-charging; 0D/1D simulations.*

1. Introduction

Nowadays, the automotive world is transitioning to cleaner technologies[1,2] in order to greatly reduce fuel consumption[3,4] and contribute less to emissions of pollutants into the atmosphere, favoring the spread of electrified vehicles. In electrified vehicles, lithium-ion batteries can work properly in a limited range of temperatures and voltages and thus, the battery management system (BMS) must ensure the battery pack's safe operation within the limits indicated by the manufacturer. Outside these limits, the performance of the cell worsens leading to several issues and dangers[5,6], such as thermal runaway for very high temperatures. When the battery temperature goes below the minimum temperature, some metallic lithium starts to deposit on the negative electrode and this causes a reduction of the batteries' life [5,7]. Excessively low temperatures lead to the breaking of the negative electrode [8,9,10].

There is plenty of literature about lithium-ion battery electro-thermal modelling, but no one proposes a generalized and complete methodology applicable to different cells and including the cell characterization, and the electro-thermal modelling. Rizk et al. [11] propose an electro-thermal nodal network for a prismatic cell: in this work the heat generation comes from an averaged value of the internal resistance of the cell. There is no characterization of the electrical parameters needed to evaluate the heat generation, which is an input for the thermal model. In the work of Dongdong Li et al. [12], the authors propose a multi-layer thermal model based on a nodal representation of a large prismatic lithium-ion cell without focusing on the characterization and modelling of the electric part. Forgez et al. [13] propose a nodal model for a cylindrical lithium-ion cell: in this case, there is no description of the characterization and post-processing of the electrical parameters. Akbarzadeh et al. [14] propose a thermal model for a high-energy prismatic lithium-ion battery cell, without investigating the internal structure of the cell, which is fundamental in order to calculate well its internal averaged thermal characteristics. Pan et al. [15] propose an electro-thermal battery model for a prismatic lithium-ion cell: to model the electrical part, an electrical second-order equivalent circuit model is used. Damay et al. [16] propose in their work a coupled electro-thermal nodal model: the electric model is based on the Randles circuits and a GITT methodology is used to find the electrical parameters of a first-order circuit. However, they do not provide any characterization analysis of the internal capacity of the cell, nor of the open circuit voltage. Makinejad et al. [17] propose an electro-thermal model for electric vehicle applications: the electrical parameters for the first-order equivalent circuit model are determined experimentally with the HPPC test; therefore, only the dependence on state of charge and temperature is detected. Xinfan et al. [18] propose a lumped-parameter electro-thermal model for cylindrical batteries: they perform a complete analysis of the electrical parameters' dependency on state of charge, temperature and current direction (i.e. charge / discharge). However, they do not consider the dependency on discharge rate. Estevez et al. [19] propose an electro-thermal model estimating all the electrical parameters and their dependencies on state of charge and temperature for the electrical part, without considering the discharge/charge effect again. This bibliography review shows that none of the previous works shows a complete li-ion characterization and modelling methodology step by step, starting from the characterization phase to the electro-thermal modelling and validation.

The novelty of this work with respect to the current literature is to propose a complete methodology for the experimental characterization and modelling of lithium-ion cells. Furthermore, this study aims to show a methodology applicable even with limited data availability: extrapolation models for capacity and electrical resistive parameters are introduced to accurately estimate value outside the tested conditions. The electrical parameters, needed for the calculation of the heat generation in the cell (electrical losses) are experimentally fully characterized. A new Hybrid Pulse Power Characterization (HPPC) protocol is proposed to determine the dependency of the electrical parameters not only on state of charge, temperature, and current direction, but also on the discharge/charge current. Models for the extrapolation of these electrical parameters at operation points other than the measured ones are developed: this allows the user to overcome possible limits of the used test bench (climatic chamber, battery tester capability). A lumped electro-thermal model has been developed within this work, where

the battery's electrical behavior is modelled with a first-order equivalent circuit model, and its thermal behavior with a nodal network. In the present work, the thermal capacity and heat generation are not assigned to the central node only but distributed with more physical meaning. The advantages of a nodal model are in its low complexity and in the lower computational cost compared with a physical model. The model has been validated in a very highly dynamic condition.

This article is divided into 7 sections. Section 2 is about the experimental tools and the characteristics of the selected cell; section 3 is about the description of the electro-thermal model; section 4 concerns the experimental characterization of the electrical parameters and the determination of thermal parameters; section 5 concerns the validation of the model; section 6 shows an off-line application of the model used to determine the thermal behavior of a battery module during ultra-fast charging; last section is about conclusions.

2. Experimental tools & selected cell

Figure 1 shows a schematic view of the cell test bench which comprises the following elements:

- Thermal chamber: it is a **walk-in climatic chamber** composed of a pre-chamber and a main chamber; the temperature range at which this room can work is between –30 ºC and 10 ºC; because this is a refrigeration chamber, it always works at lower temperature than the ambient temperature[20].
- Battery Tester Emulator **LBT21044-0~10V-100/10/1/0.1A-4CH-380V3P**: this battery tester from Arbin is composed of 4 channels (each channels provides up to 100 A and 10 V) with the possibility to connect the channels in parallel to increase the current when necessary; with a voltage resolution of ~1μV, a voltage control accuracy of ±2 mV, and a current control accuracy of ±20 mA for a range of currents of 10 A, it offers the right measurement accuracy for the battery testing[21].
- Data acquisition system consisting on a **Agilent 34972A**: speeds of up to 600 readings per second on one channel and scan speed of up to 250 channels per second; selection of multiplexing, matrix, general purpose Form C switching, RF switching, digital I / O, totalization, and 16-bit analog output functions[22].
- Thermographic camera **ThermaCAM™ P60**, with a thermal sensitivity of 0.06 °C at 30 °C, an image frequency of 50/60 Hz non-interlaced, 640 x 480 pixels, full color [56].
- Thermocouples: 1-mm **type K** thermocouples for the surface temperature measurement and self-adhesive polyimide type K thermocouple for the terminals.
- Holder: in-house realized to hold steady the cell during the test activities.

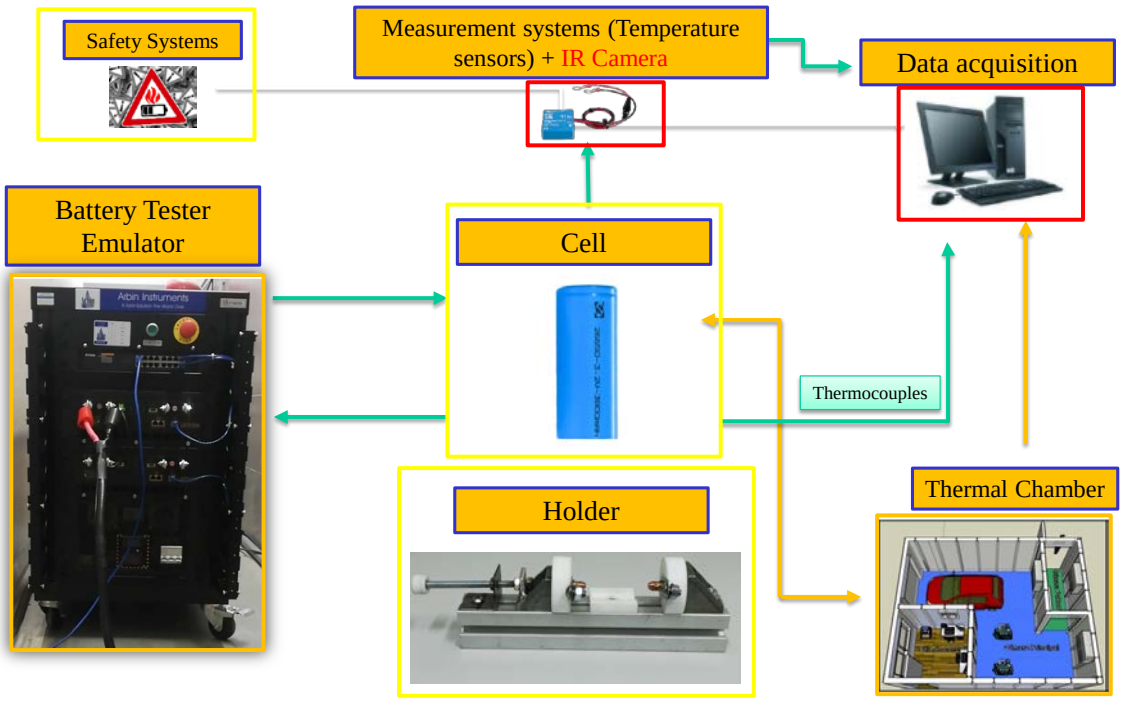

Figure 1: Test bench for the cell characterization

The main characteristics of the cell used for this analysis are listed in table 1 [23].

Table 1: Characteristics of the analyzed cell

Format	26650 cylindrical
Chemistry	LFP
Nominal voltage [V]	3.2
Nominal capacity [Ah]	3.8
Discharge cut-off voltage [V]	2.5
Charge cut-off voltage [V]	3.65
Discharge temperature range [°C]	[-20;60]
Charge temperature range [°C]	[0;55]
Storage temperature range [°C]	[-20;55]
Weight [g]	87.5
Diameter [mm]	26
Length [mm]	65

3. Model description

The global model of the cell considers both the electrical and the thermal parts. Both are connected to each other: the electrical model needs the cell temperature to estimate the electrical parameters, while the thermal model requires the value of the generated heat to determine the temperature, as shown in the figure 2 [15].

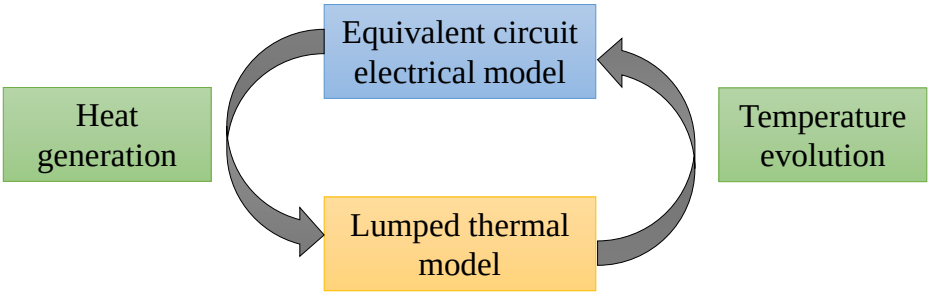

Figure 2: Structure of the electro-thermal model

3.1 Electrical model

The **equivalent circuit** approach is used in this work to model the electrical behavior of the cell. These models are based on electrical circuit analogies, that simulate the real behavior of the voltage delivered at the terminals of a cell, when it is stimulated with an input current [24]. Therefore, there is no need for deep knowledge of the electrochemical, diffusion and mass transport phenomena happening inside the cell.

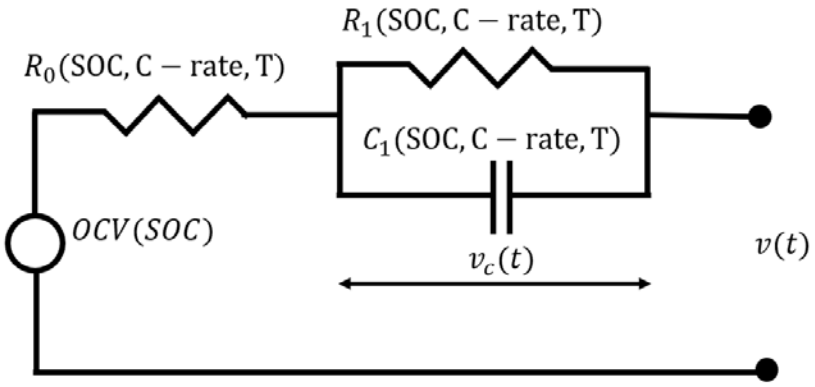

Figure 3: First order equivalent circuit model

The main difference between a zero and a more-than-zero equivalent circuit model is that the former can adequately explain the behavior of the cell only during a rest, or during the instantaneous voltage drop (or rise) due to the application of current, whilst the latter can also accurately simulate the voltage variation during the whole interval in which the current is applied [24]. A first order equivalent circuit model has been chosen for this analysis. In this kind of model, there are 4 elements:

- The *open circuit voltage source* $OCV = f(SOC)$: it considers the voltage that the cell delivers when it is **unloaded** and in a balanced condition [24]. The open circuit voltage has a one-to-one correspondence with the state of charge of the cell [25]. Hence, to adequately estimate the open circuit voltage of a cell, it is necessary to determine opportunely the SOC of the cell. In the literature there exist several state of charge estimation algorithms, each with its own advantages [26], [27]. In this work the **coulomb counting method** is chosen [27]:

$$SOC = SOC_0 - \frac{1}{C_{Ah}} \int_{t_0}^{t} \eta I dt \qquad (1)$$

where:

- SOC_0 is the starting value of the state of charge at time t_0;
- C_{Ah} is the current value of the capacity of the cell (it can differ from the rated value);
- η is the coulombic efficiency that is equal to 1 in discharge, and is less than 1 during charging operations [27]; in this case, the coulombic efficiency has been fixed equal to 1 both in charging and in discharging operations;
- I is the intensity at which the cell is charged or discharged.

The accuracy of the state of charge estimation depends on the precision of the above-mentioned parameters and on the precision of the current sensor. Once the state of charge is estimated, the right open circuit voltage value is extrapolated using the maps from the experimental characterization of the parameter.

- The *ohmic resistance* $R_0 = f(SOC, c-rate, T, sign(I))$: when the cell is connected to a load, it undergoes an instantaneous voltage drop during discharging (or voltage rise during charging). This phenomenon is considered with this resistive parameter. Physically, it represents the ohmic losses happening inside the terminals and liquid phase in the cell [28];
- The *polarization resistance* $R_1 = f(SOC, c-rate, T, sign(I))$ and the *polarization capacitance (*or *double-layer capacitance*) $C_1 = f(SOC, c-rate, T, sign(I))$: these two parameters take into account the polarization losses happening inside the cell due to charge transfer and diffusion phenomena [24]. Look-up tables of resistive and capacitive parameters are provided by the experimental campaign carried on for the analyzed cell.

The equations implemented in the model are the following [29]:

$$v(t) = OCV\big(SOC(t)\big) - v_c(t) - R_0 I(t) \tag{2}$$

$$\frac{dv_c(t)}{dt} = \frac{1}{C_1}\left(I - \frac{v_c(t)}{R_1}\right) \tag{3}$$

where:

- v is the terminal voltage of the cell
- v_c is the voltage at the terminals of the capacitor.

3.2 Heat generation model

According to the literature, it can be assumed that the heat generation in a cell is given by the sum of three terms [30,31]:

$$\dot{Q} = I \cdot (V - OCV) + I \cdot T\frac{\partial OCV}{\partial T} - \sum_i \Delta H_i^{avg} r_i - \int \sum_j \left(\overline{H_j} - \overline{H_j}^{avg}\right)\frac{\partial f_j}{\partial t} du \tag{4}$$

where:

- ΔH_i^{avg} is the entropy variation associated with the *i*th reaction considering an average concentration in the volume [30]

- r_i is the reaction rate
- $\overline{H_j}$ is th molar entropy of the *j*th piece of the battery
- $\frac{\partial f_j}{\partial t}$ is the variation of the ion concentration in the *j*th piece of the battery over time
- u is the volume.

Equation (4) is composed of 4 terms:

- The first term of the right-hand side indicates the heat generated from resistive dissipation; it is always positive and is **irreversible**. In this work, maps of the electrical parameters are used to estimate this term.
- The second one is a **reversible** entropic term that can be either positive or negative. The value of the derivative of the voltage with respect to temperature is available in the literature for a similar chemistry to the one chose for this work.
- The third term represents the heat produced or consumed by any chemical reaction that may occur in the cell, and it can be positive or negative. This term indicates the ageing processes happening inside the cell, and they are neglected in this case.
- The last term represent the **heat of mixing** and it is due to concentration gradients in the cell. This term is usually neglectable because in a system with good transport properties, these gradients are very limited.

Hence, in this work, the heat generation is expressed as:

$$\dot{Q} = \dot{Q_{irr}} + \dot{Q_{rev}} \tag{5}$$

3.3 Thermal model

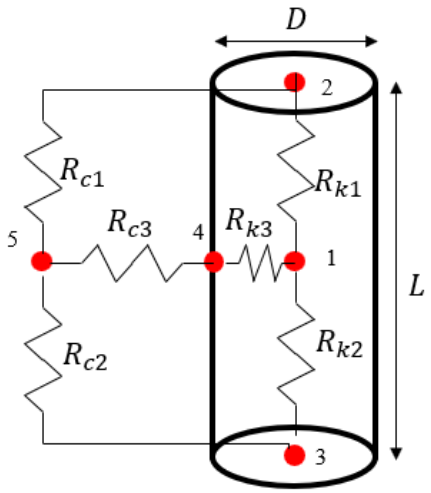

Figure 4: Nodal thermal model

A lumped thermal model has been chosen to analyze the thermal evolution in the cell used for this work. Like the equivalent circuit model, the nodal thermal model is based

on an electrical circuit analogy. In this case, the heat flowing through the nodes of the model is associated to the current flowing in an electrical circuit. There is a similarity between the electrical current created by a voltage gradient and the heat generated by a temperature gradient [16]. The heat generation, estimated thanks to the knowledge of the electrical parameters, is the only input to the model. A volume, a composition and a thermal capacity are associated to each node. Inside the battery, the heat flux circulates from node to node by conduction, while on the outer surfaces of the battery, it is a convection process that occurs from a surface cell node to the surrounding air. The heat transfer by radiation is neglected in this analysis since the surface temperature of the cell is low.

The developed lumped thermal model for the cylindrical cell is shown in Fig. 4. It is composed of four cell nodes and one external node:

- the **internal** node: the active zone of the cell, i.e., the jellyroll composed of several layer of anode, cathode, separators soaked into the electrolyte is represented by this node.
- the two **terminals** nodes: for each one of the terminals (positive and negative) one node is considered.
- the **surface** node: this node contains the whole external casing of the cell.
- the **air node**, representing the air surrounding the cell.

The heat generated as an output from the electrical and heat generation models (eqs. 1 to 5) is partly assigned to the internal node (node 1) and partly to the terminals nodes (nodes 2 and 3) according to the distribution proposed in Nazari et al [31]; that is, for a cell whose capacity is between 2 and 8 Ah, about 96-97% of the heat goes to the core and the remaining to the terminals.

As previously stated, by estimating volumes, materials and internal composition of each node, a thermal capacity term is assigned to each node.

For a solid generic node, the thermal balance can be written as follows:

$$m_i c_i \frac{T^i_{t+\Delta t} - T^i_t}{\Delta t} = \sum_j K_{ij}(T^j_{t+\Delta t} - T^i_{t+\Delta t}) + \sum_k Q_{k\to i} + \sum_j h_{ij} A_{ij}(T^l - T^i_{t+\Delta t}) \quad (6)$$

where:

- $m_i c_i$ represents the thermal capacity of the generic node, product of the node mass and heat capacity.
- K_{ij} the thermal conductance between the node i and the node j: for linear geometry, $K = \frac{kA}{L}$; for cylindrical geometry, $K = \frac{2\pi kL}{\ln(r_2/r_1)}$ with k the thermal conductivity, L the length of the cylinder, r_1, r_2 the internal and external radii of the geometry respectively.
- $Q_{k\to i}$ the generic source of heat generation inside the control volume of the node.
- h_{ij} the heat transfer coefficient with the fluid j.

To solve this equation, an **implicit** formulation is used. Its advantage over the explicit form is that the solution is unconditionally stable, which is particularly interesting when

simulating transient behavior, which is the case in this work. On the other hand, the implicit form tends to be computationally more time consuming.

Rearranging for all the nodes of the analyzed system, a matrix expression is obtained [32]:

$$[T^t] = ([K] - [C])^{-1}([T^{bc}] - [C][T^{t-\Delta t}]) \quad (7)$$

where:

- $[T^t]$ is the vector of the node temperatures in the current instant
- $[K]$ is the conductance matrix
- $[C]$ is the capacitance matrix
- $[T^{bc}]$ is the vector of the boundary conditions, including not only temperatures, but also generated heat
- $[T^{t-\Delta t}]$ is the vector of the node temperatures in the last-but-one instant.

For a steady state kind of problem, the transient term is equal to 0 and the equation simplifies to eq. (8) [32]:

$$[T^t] = [K]^{-1}[T^{bc}] \quad (8)$$

The identification of the thermal parameters included in the conductance and capacitance matrices is discussed in the next section.

4. Parameters' identification

In order to determine the electrical parameters of the above-mentioned first-order equivalent circuit model an experimental campaign was carried out. The electrical parameters that had to be characterized are the following:

- $C_{Ah} = f(T, c-rate)$: the *cell capacity*, which will affect SOC as Eq. (1) shows, is expressed in Ah, and it varies in function of the temperature and of the electric current. To have a precise mapping of this parameter, **capacity tests** were carried out at different temperatures and discharge rates.
- $OCV = f(SOC)$: the open circuit voltage, which will affect directly the terminal voltage as Eq. (2) shows, has been determined by running **OCV tests**.
- $R_0, R_1, C_1 = f(SOC, T, c-rate, sign(I))$: the ohmic resistance R_0, the polarization resistance R_1 and the polarization capacitance C_1, are determined by running **HPPC** tests [33].

4.1 Capacity identification

The capacity test consists in a complete discharging of the cell starting from the maximum voltage until the cut-off discharge voltage. In this case, the whole test, shown in fig. 5, consists of three stages:

- charge of the cell using the CCCV protocol (charging the cell at 1C up to the maximum voltage and, once achieved this condition, holding the voltage fixed and letting the current go down until a cut-off condition is satisfied)
- rest of half an hour
- discharge at the chosen rate of discharge.

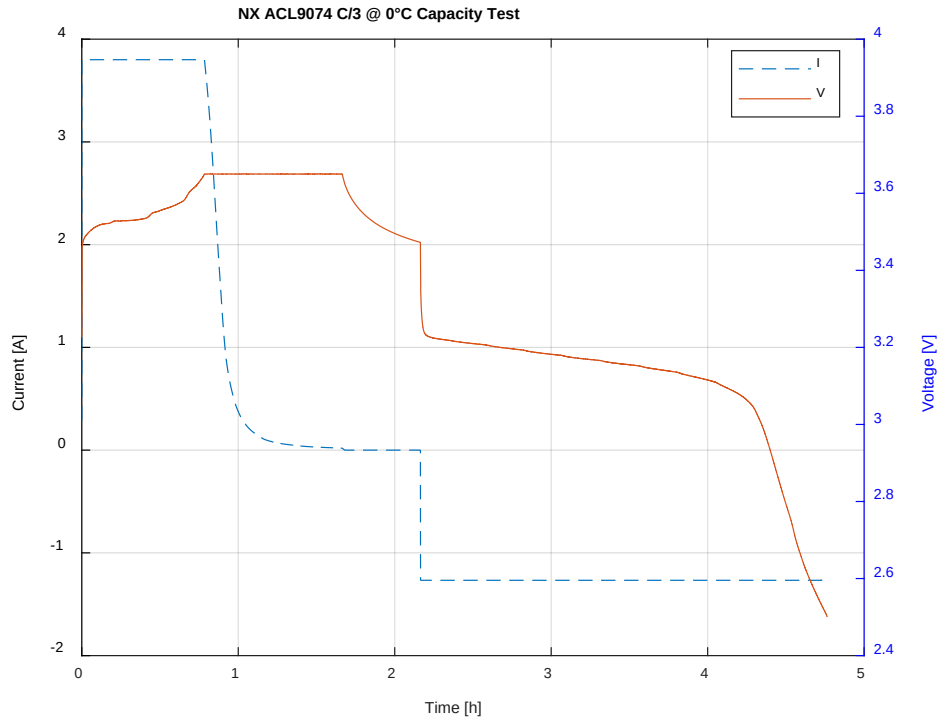

Figure 5: Example of capacity test at 0°C

Considering the limits of the climatic chamber used to carry out the experimental characterization campaign and the limiting characteristics of the cell, this test was repeated at 5 discharge rates ($C/5$, $C/3$, $C/2$, $1C$, $2C$) and two temperatures ($0, 10$°C).

The results of the capacity tests are summarized in figure 6.

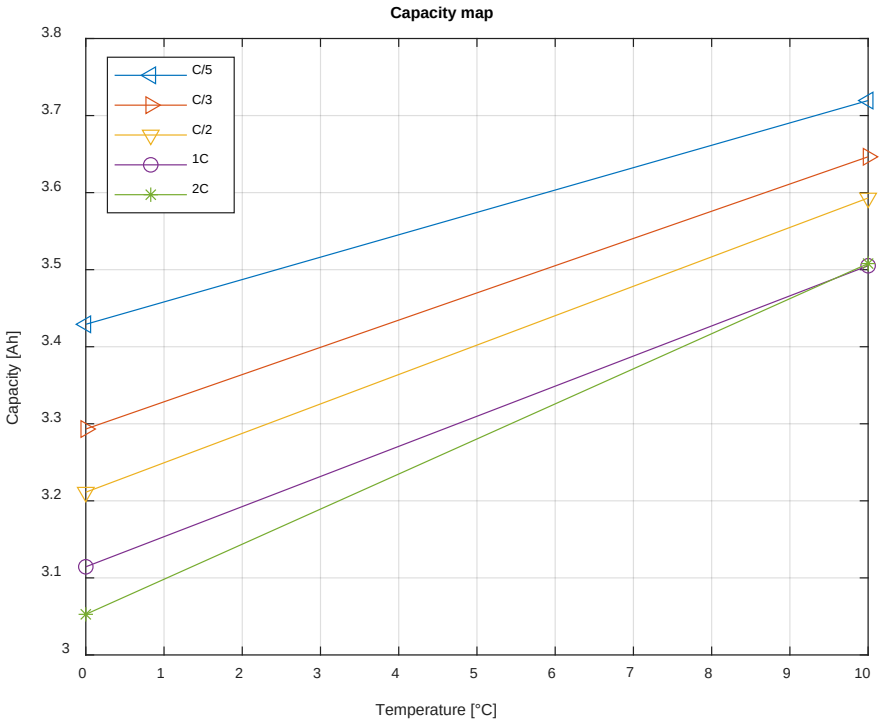

Figure 6: Capacity test results

Regarding the dependency of the capacity on temperature, as is widely discussed in the literature [34,35] , the lower the temperature, the lower is the available capacity extracted from the cell. The main reason is that when a lithium-ion cell is discharged at low temperatures, all the diffusion phenomena inside the battery are held back. This effect contributes to increasing the charge transfer resistance between the liquid and the solid phases [35]. Instead, as seen in several studies [36,37], , the charge transfer resistance is a function of the constant charge transfer rate and this parameter is inversely proportional to the temperature.

Regarding the dependency of the cell capacity on the C-rate, it is generally observed that the capacity tends to decrease as the discharge rate increases. This phenomenon is analyzed by Peukert's law [38], [39]:

$$I^{PC} \cdot \Delta t = constant = C_n \tag{9}$$

where:

- Δt is the time expressed in hours.
- PC is the Peukert Coefficient, which for lithium-ion cells is greater than 1. It considers the losses ocurring inside the cell when it is discharging. These losses are higher when the cell is discharged at higher C-rates because the higher the C-rate is, the lower the number of active sites in the electrode is and, consequently, the greater is the charge transfer resistance.
- C_n is the nominal capacity, i.e., the capacity given by the manufacturer.

Finally, to extrapolate the cell capacity values at other temperatures than the measured ones, the Galerkin et al. model is used [38]:

$$C = C_{ref} K \cdot \frac{(\frac{T - T_L}{T_{ref} - T_L})^{\beta}}{(K-1) + (\frac{T - T_L}{T_{ref} - T_L})^{\beta}} \tag{10}$$

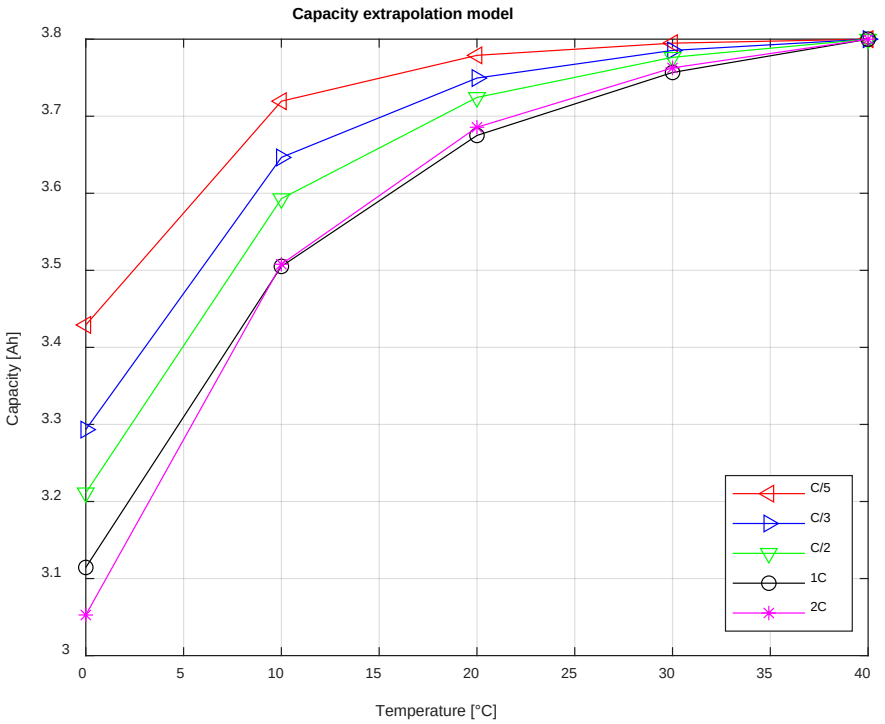

Figure 7: Results of the capacity extrapolation model

where:

- T_{ref} is the reference temperature for the cell.
- C_{ref} is the nominal capacity extracted at T_{ref}.
- T_L is the temperature at which no capacity can be extracted from the cell, i.e., $C = 0$: this parameter is found to be about 240 K in the literature.
- K is a parameter that consider the increase in capacity in function of the temperature increase within the thermal operating range of the cell.
- β is an empirical constant.

4.2 OCV identification

To get the $OCV - SOC$ curves in charge and discharge, an OCV test is performed. In the literature, there are several examples of procedures to perform this test ([40], [25]) but, basically it consists in the following stages:

- a full charge of the cell at 1C according to the CCCV protocol, followed by a 3-hours rest;
- then, a series of 10% discharge phases of the cell, alternating with 3-hours rests are carried out until the battery is completely discharged.

In the same way, the battery is recharged by alternating 10% of cell recharging with 3-hours rests until the cell is fully charged. The points selected for the open circuit voltage curve are those at the end of each 3-hours' rest periods, as it is considered that the battery has then reached a state of equilibrium.

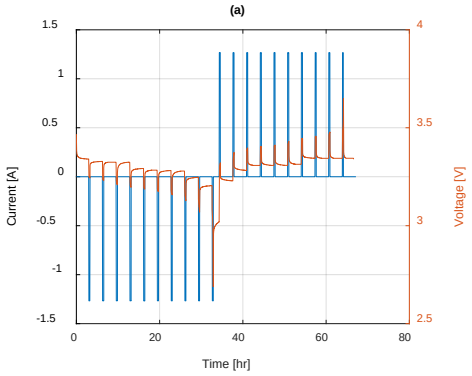

Figure 8: OCV test results

Figure 8 presents the results obtained for the OCV-SOC curves in charge and in discharge: in Figure 8a the previously described test protocol is shown; in Figure 8b the SOC variation due to discharge and charge pulses is shown; in Figure 8c, the OCV points extraction procedure is shown (the voltage at the end of the rest period is selected as balanced voltage, that is an OCV curve point); in Figure 8d the discharge and charge OCV-SOC curves are shown.

4.3 Electrical parameters identification: R_0, R_1, C_1

The electrical parameters of the first-order equivalent circuit model were determined by performing an HPPC test [41], a test defined in the Idaho National Laboratory manual. However, for this work, a new protocol has been elaborated: in fact, the original HPPC test [41] foresees pulses only at 1C, thus allowing to have information only at a discharge rate; in the new protocol, on the other hand, the cell undergoes charge and discharge pulses at various charge and discharge rates within the limits of the operating window of the cell.

The HPPC protocol developed for testing the cell is presented in Fig. 9 and it consists of:

1. an initial charge at 1C according to the CCCV protocol
2. 1-hour rest
3. a discharge of 10% of the cell capacity at 1C
4. 1-hour rest
5. pulse train at the corresponding SOC level (Fig. 10): discharge pulses at C/5, C/3, C/2, 1C and 2C are considered; charge pulses at C/5, C/3, C/2 and 1C are

considered. The charge and discharge rates are chosen according to the charge/discharge rate limits indicated by the manufacturer of the cell.

The steps 3 to 5 are repeated until the cell is completely discharged.

The test has been run at 0 and 10°C, so that information at different C-rates, SOC stages and temperatures is available to calibrate the electrical parameters of the model.

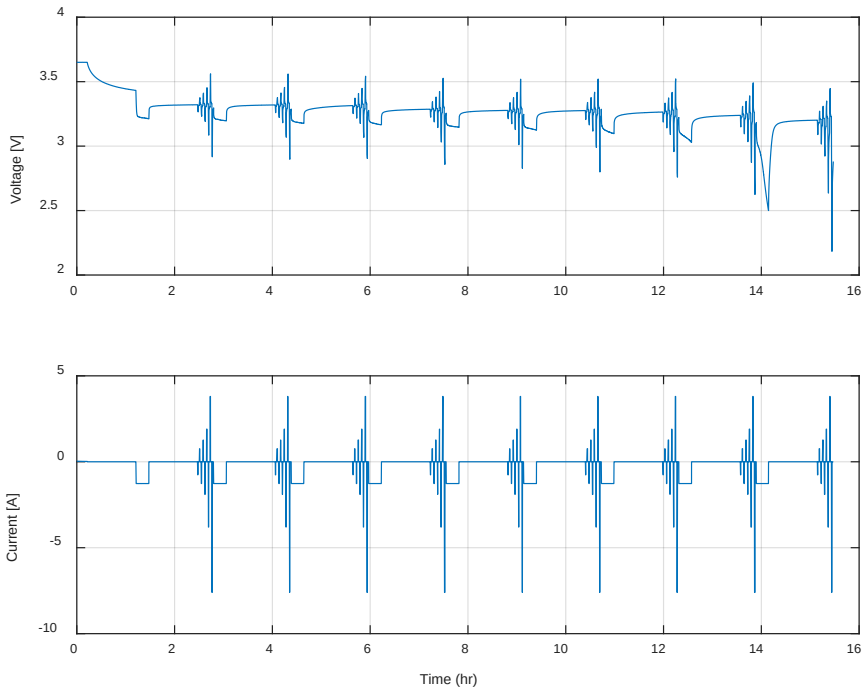

Figure 9: HPPC test protocol

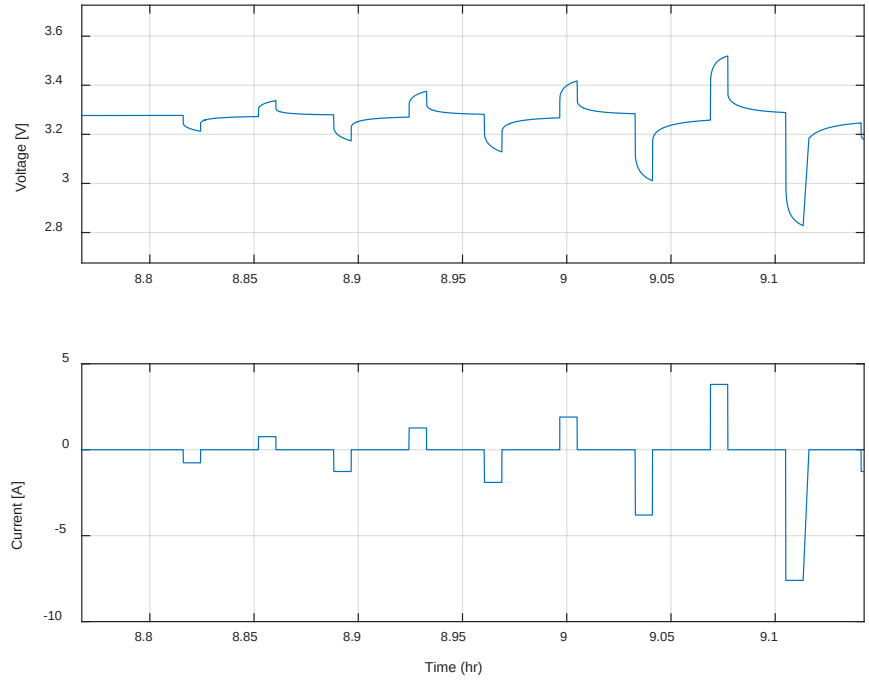

Figure 10: Pulse train

To get the electrical parameters from the HPPC data, a **step-method** is considered. A resistive parameter can be estimated considering a variation of the battery voltage versus the current applied, as indicated in the Idaho Laboratory Manual [33,41]. For a first-order equivalent circuit model, the ohmic resistance R_0 is modeled considering the immediate variation in the voltage response; the charge transfer resistance R_1 is modeled considering the remaining part of the pulse voltage variation. In this case, an algorithm of optimization was used considering fixed the ohmic resistance R_0 and the open circuit voltage OCV and tuning the polarization resistance and capacitance R_1 and C_1, as shown in Fig. 11.

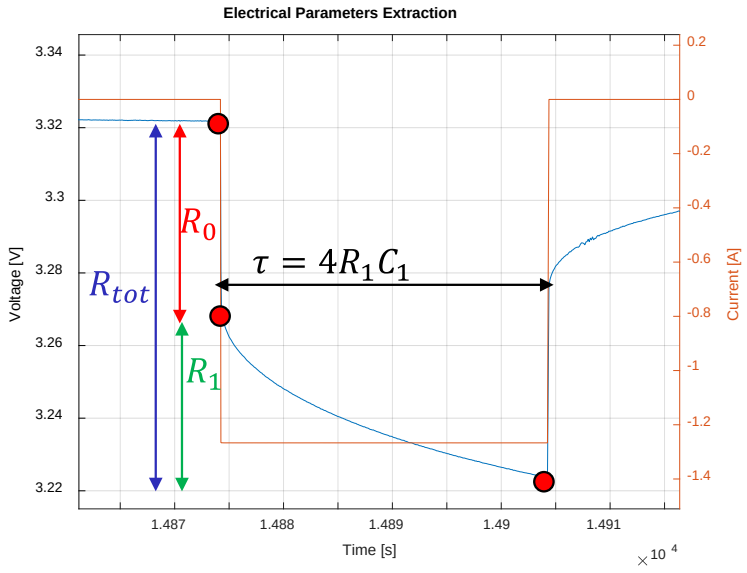

Figure 11: Step method for electrical parameter extraction

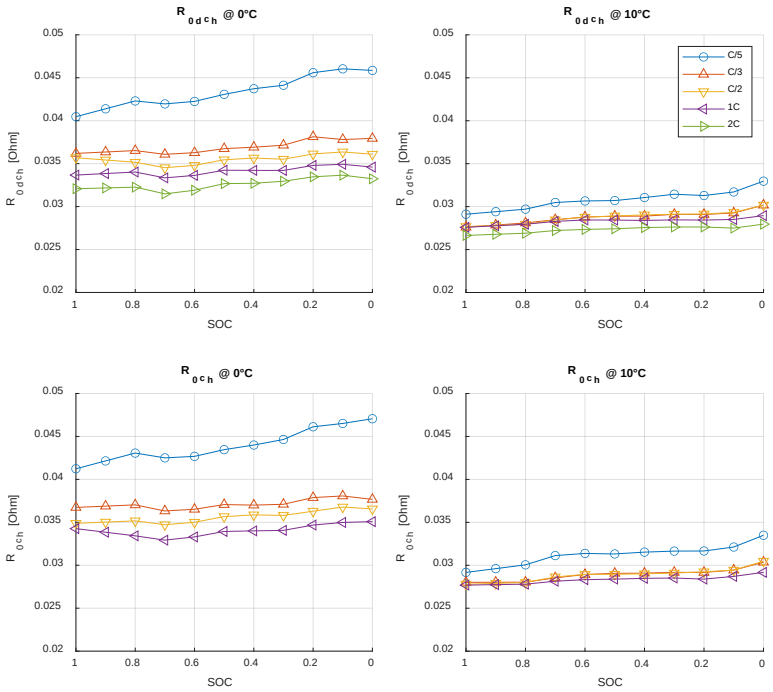

Figure 12: Ohmic resistance (R_0) in charge and discharge from HPPC test @ 0-10°C

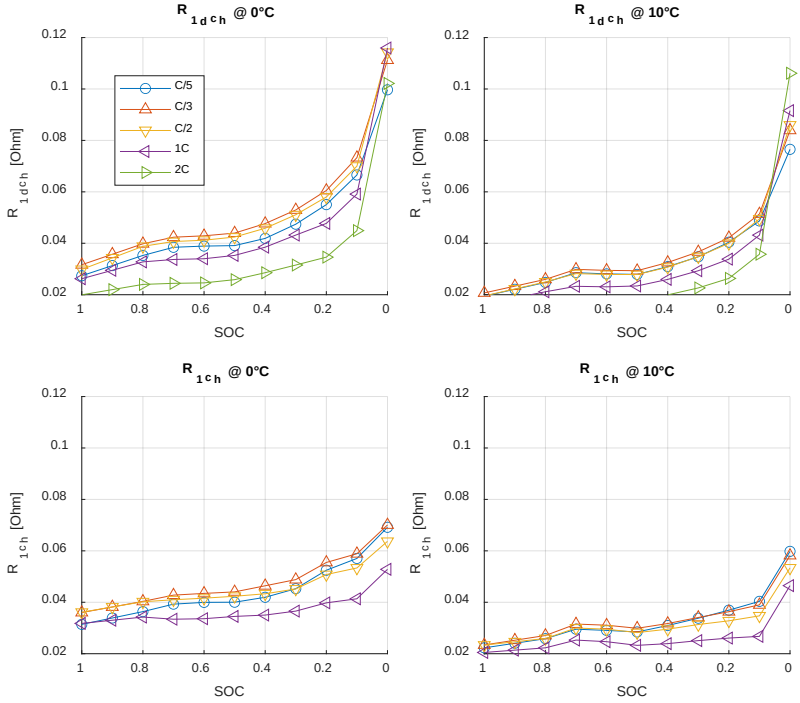

Figure 13: Charge transfer resistance (R_1) in charge and discharge from HPPC test @ 0-10°C

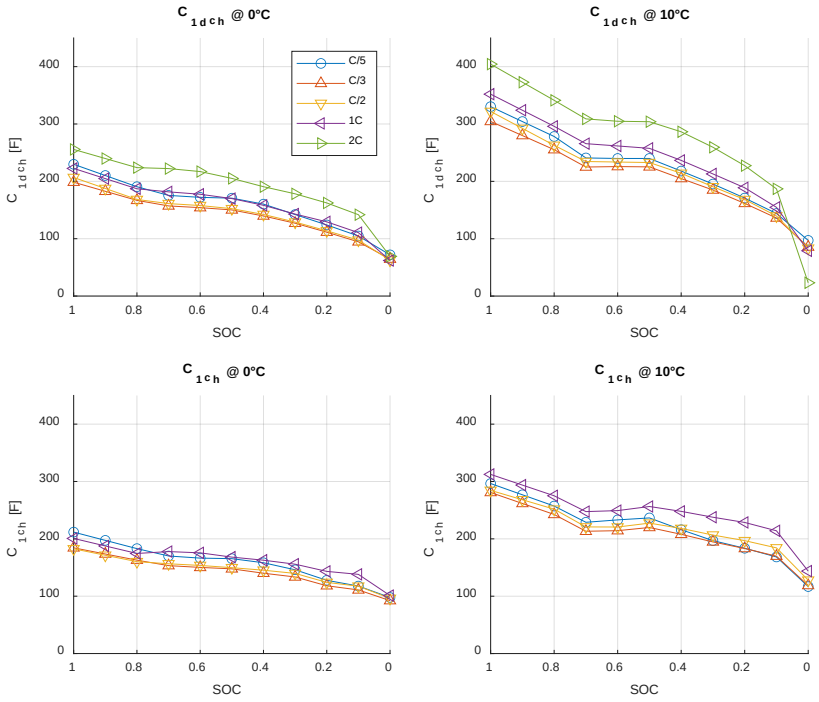

Figure 14: Double layer capacitance (C_1) in charge and discharge from HPPC test @ 0-10°C

In figure 12 to 14, the electric parameters obtained from the post-processing of the data are shown. For both resistances (R_0 and R_1), the values at the two chosen temperatures (0 and 10°C) during charge and discharge, are plotted. Both the ohmic resistance, R_0 , and the charge transfer resistance, R_1, decrease in function of the SOC; furthermore, the higher the discharge/charge rate is, the lower the resistances are. Of course, when increasing the temperature, the resistances decrease with an Arrhenius shape. An extrapolation model is needed to obtain the values of the cell capacity, and of the electrical parameters at other temperatures. In particular, as shown in the literature [42], the behavior of the resistive parameters in function of the temperature follows the Arrhenius' law:

$$R_i = A_f e^{-\frac{E_a}{RT}} \tag{11}$$

where,

- A_f is the pre-exponential factor
- E_a is the activation energy of the reaction.

Once these two parameters are calibrated for every SOC and C-rate analyzed, it is possible to deduce the values of the resistive parameters at temperatures other than those that could be tested.

4.4 Thermal parameters identification

The thermal parameters that must be determined for the lumped thermal model are:

- thermal capacity of the cell

- internal conductive resistances between nodes

- external convective resistances from node to air

These parameters were determined using internal geometric characteristics and thermal characteristics found in the literature.

Once hypotheses have been made about the internal structure of the cell and having assigned to each of the model nodes its corresponding volume and composition, it is possible to calculate the thermal capacity of each node. Considering the jelly-roll composition of the active zone of the cell (Fig. 15), the thermal capacity of the model internal node is calculated as a weighted average of the characteristics of each of the materials inside it, listed in table 2 [43].

Table 2: Thermal characteristics of the jelly-roll materials

	Material	*Specific heat [J/kg*K]*	*Density [kg/m3]*	*Volume (mm3)*
Positive current collector	Aluminum	903	2700	1460.7
Cathode Electrode	LFP	1260.2	1500	12415.95
Separator	PP/PE/PP	1978	492	2337.12
Anode electrode	Graphite	1437.4	2660	14607
Negative current collector	Copper	385	8900	730.35

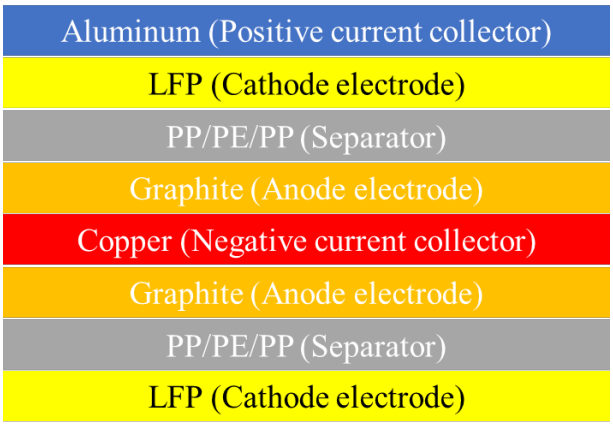

Figure 15: Schematic of the internal structure of the jellyroll of the cell

Finally, the thermal capacity is calculated for each node knowing the materials of the terminals and of the casing.

For the calculation of the internal conductive resistances, the thermal conductivity of the material composing the cell must be known, as well as some internal characteristics of the cell, such as porosity of the layers and thermal conductivity of the electrolyte. In fact, according to the work of Cheng et al. [44], the thermal conductivity of the generic material i composing the jellyroll depends on the porosity of the layer ε and on the thermal conductivity of the electrolyte K_{el}. As shown in various studies [44,45], the porous material can be modeled as a material with no pores put in parallel with a volume of air. Considering the global thermal resistance of this parallel configuration, equation (12) is found:

$$k_i = k_m \cdot (1 - \varepsilon) + k_{el} \cdot \varepsilon \tag{12}$$

where:

- k_i is the thermal conductivity of the layer in the active zone taking into account the effect of the porosity and of the electrolyte
- k_m is the thermal conductivity of the layer without correction.

Once the thermal conductivity of any layer is obtained, the thermal conductivity in any of the three axes is calculated considering the anisotropy of the system [43]:

$$k_{rad} = \frac{ln\,(\frac{r_N}{r_0})}{\sum_{i=1}^{N} \frac{ln\,(\frac{r_i}{r_{i-1}})}{k_i}} \tag{13}$$

$$k_{ax} = \sum_{i=1}^{N} k_i \frac{r_i^2 - r_{i-1}^2}{r_N^2 - r_0^2} \tag{14}$$

where k_{rad} , and k_{ax} refer to the thermal conductivity calculated in the radial direction of the cell, respectively axial, and r_i refers to the i-th layer of the cell's jelly-roll. With the known internal structure and thermal conductivity of the cell, the internal conductive resistances can be determined.

The heat transfer coefficient to the surrounding air is needed to calculate the external convective heat transfer. A value $h = 12\ W/m^2K$ has been determined by adjusting the model output to fit the experimental measurement of the cell temperatures.

5. Model validation

Once the lithium-ion cell has been characterized and all the electrical and thermal parameters of the electro-thermal model have been determined, it is possible to validate the model. In order to validate the model, an highly dynamic real driving emissions (RDE) cycle has been chosen. The RDE used in this work has been generated in-house according to current normative and legislations. The RDE cycle and the results of the electrical and thermal validation are shown in Figures 16. The initial conditions at which the validation test is carried on are the following one:

- Ambient temperature is set equal to 20,5°C;
- Initial state of charge of the cell set equal to 0.5.

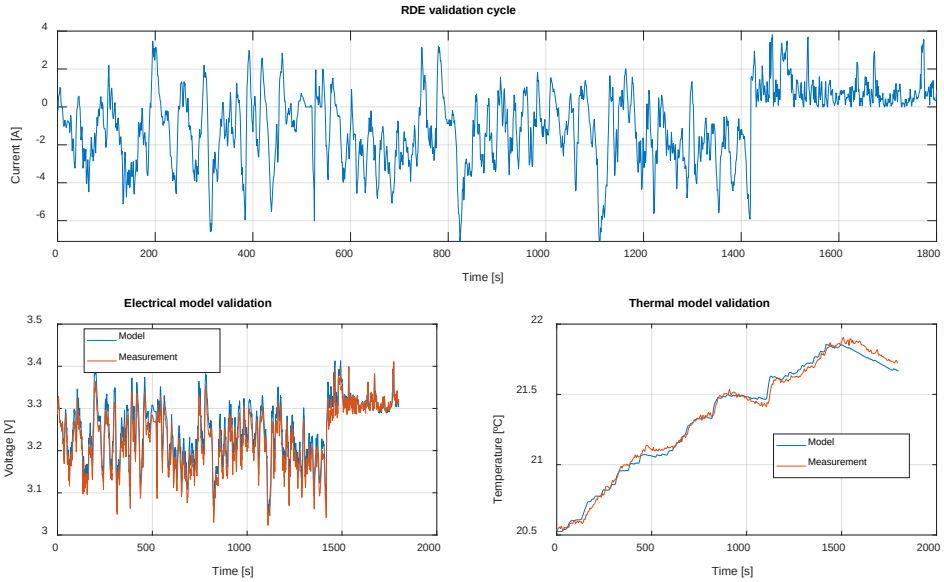

Figure 16: Validation cycle and electrical and thermal models' validation

The errors of the electrical model and of the thermal model are shown in Figure 17. The model captures accurately the temporal variation of the cell surface temperature recorded during the measurement, as well as the electrical behavior of the cell in terms of terminal voltage.

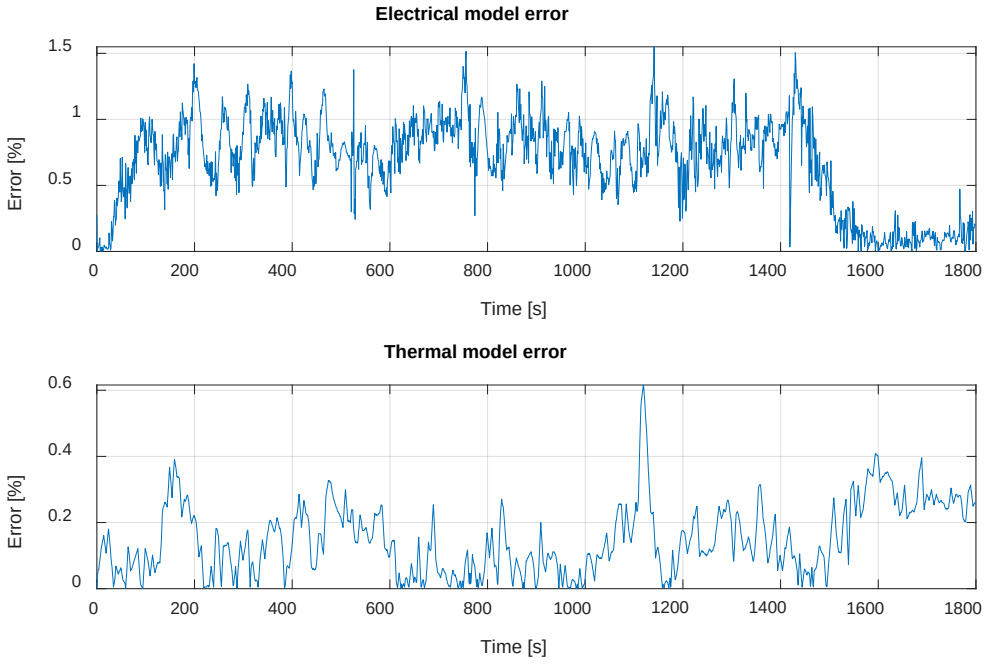

Figure 17: Electrical and thermal models' errors

The model shows a good agreement with the measurement in this highly dynamic condition both in the electrical part, and in the thermal part.

6. Module thermal analysis during fast charging

One of the hot topics in research about lithium-ion batteries is that of fast or ultra-fast charging. For the performance of a lithium-ion battery, several operational and environmental factors must be considered: rate of discharge / charge, temperature, state of charge, maximum voltage, minimum voltage, etc. The operating window of a battery is defined by the combination of the range of temperature, current, and voltage within which a battery can work safely. As the ambient temperature decreases, the charge rate must be kept low. For this reason, the temperature can be considered already a limit for the fast charging [37].

Among the most critical problems that lithium-ion batteries face during operations at low temperature is the lithium plating, as this phenomenon leads to a rapid capacity loss. The lithium metal becomes isolated from the anode surface, and this can cause a short circuit situation. During charging operations, this problem increases significantly when the temperature decreases. In general lithium plating is reported to be very significant at low temperatures, but in the case the battery has been charged at very high C-rate, lithium plating can occur also at higher temperatures than 25 ° C [37] .

The validated lumped thermal model gives the possibility to simulate a whole range of operating conditions, including those that may present a risk if implemented physically. It has therefore been used here to study the thermal evolution of the standalone cell and of the cell in a battery module for normal and ultra-fast charging conditions.

A configuration of sixteen cylindrical cells packed in a battery module has been considered. Due to the symmetry of the problem and assuming that the behavior of all cells is the same, the study can be simplified to a sub-module composed of 4 cells, as shown in Fig. 18.

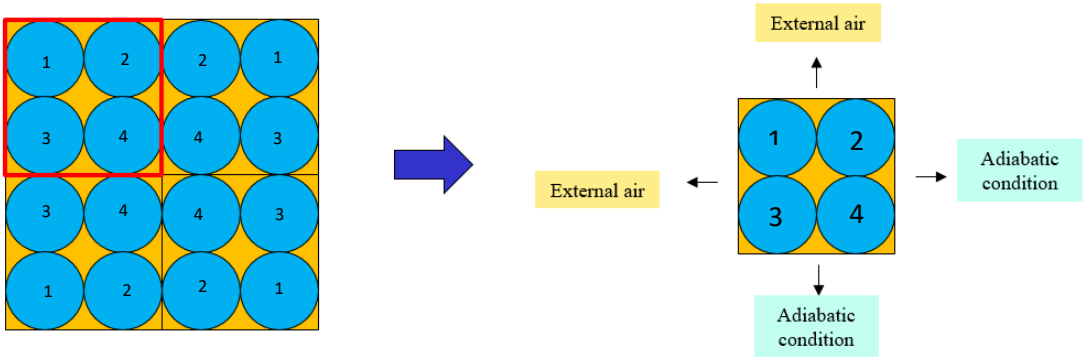

Figure 18: Module configuration

Each of the four cells exchanges heat by convection with the air inside the module (yellow area in Fig. 18); along the two non-adiabatic faces, there is no heat transfer at all. The module is assumed not to be cooled by a refrigerant and in contact with air only. This study is aimed at observing the temperature evolution inside the module configuration, not only for the cells, but also for the air inside the module, to highlight the impact of the module configuration on the thermal evolution, as compared to the stand-alone cell.

The initial temperature is 0°C and the heat transfer coefficient is estimated at $h = 12 \frac{W}{m^2 K}$. The 2D nodal network used for this analysis is shown in figure 19: for each of the four

cells the surface node transfers heat by convection to the air inside the module. A volume and a thermal capacity have been assigned to each internal air node. The model is therefore composed of 18 nodes: 8 cell nodes, 9 internal air nodes and 1 external air node:

- *EA* stands for external air node
- *A-nn* stands for internal air node
- *-S* indicates a surface node
- *-C* indicates a core node

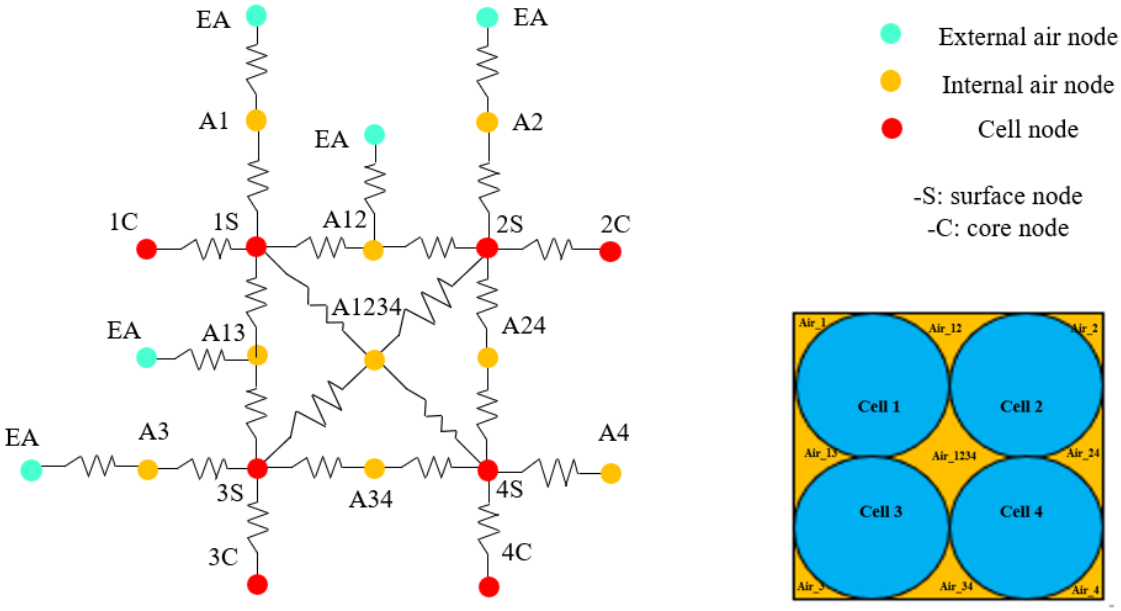

Figure 19: 2D Nodal network for the module

The temperature evolution of the stand-alone cell is compared to that of the module configuration for a 1C charging process in Fig. 20, and for the most critical situation, a complete ultra-fast charging of the cells at 6C in Fig. 21.

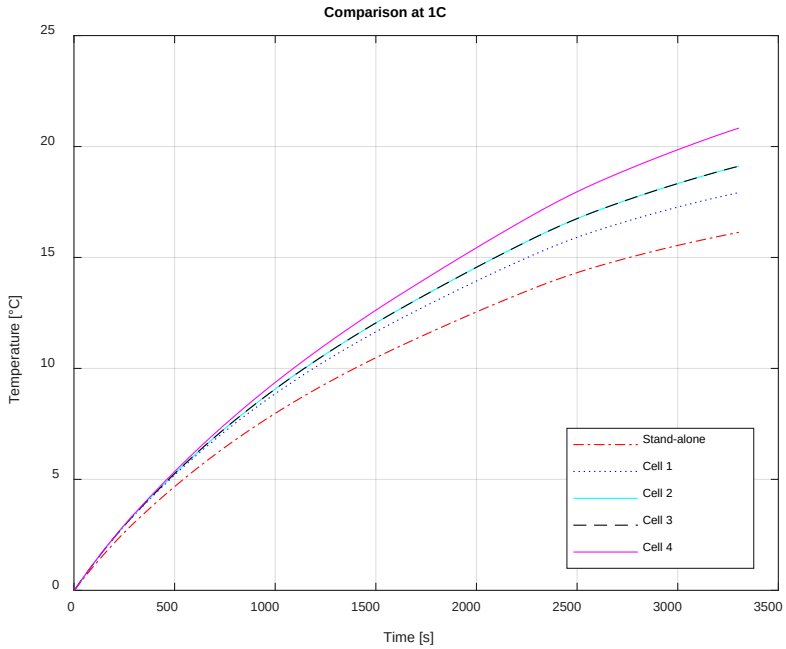

Figure 20: Thermal evolution during 1C charging

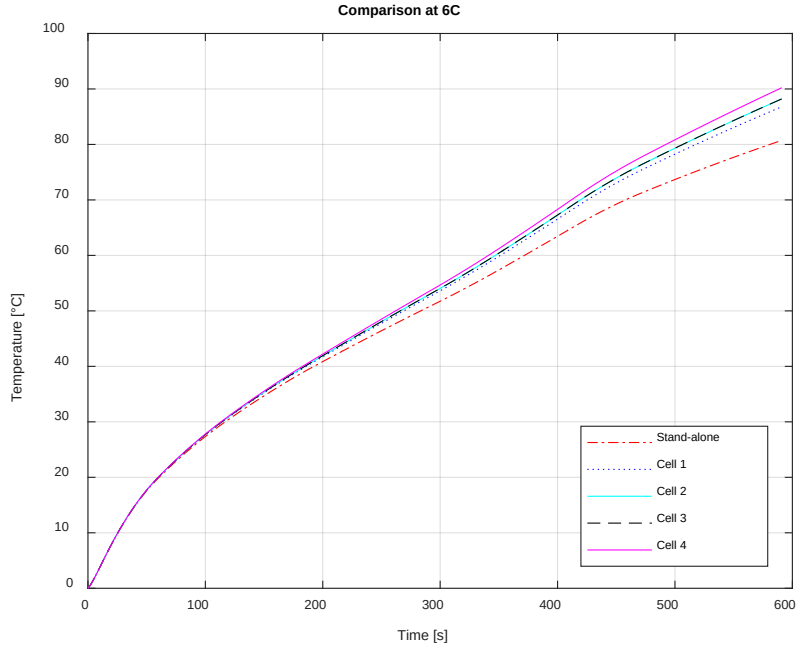

Figure 21: Thermal evolution during 6C ultra-fast charging

All the cells in the module have higher temperatures than the stand-alone cell during most of the charging process, with a difference of almost 10°C at the end of the 1C charging process between the stand-alone cell and the hottest cell in the module configuration, cell 4 as shown in Fig. 20. Within the module itself, the cells reach different temperatures: the innermost cell 4 shows the highest temperature, while the outermost cell 1 has the lowest. This clearly demonstrates that the module inner cells are the most hazard prone. The

average temperature they may attain during charging will limit the C-rate at which the module may be charged, and also reduce their life-span [51].

The upper limit temperature guaranteed by the manufacturer for a lithium-ion cell is usually around 55-60ºC. Hence, the results in Fig. 21 confirm that it is impossible to fully recharge a cell with fast and ultra-fast charging without any adequate thermal management system. Indeed, according to the results of the model simulations, the cell and module can only be partially charged in 6C ultra-fast charging conditions during a maximum of about 5 minutes, otherwise there is a risk of lithium plating.

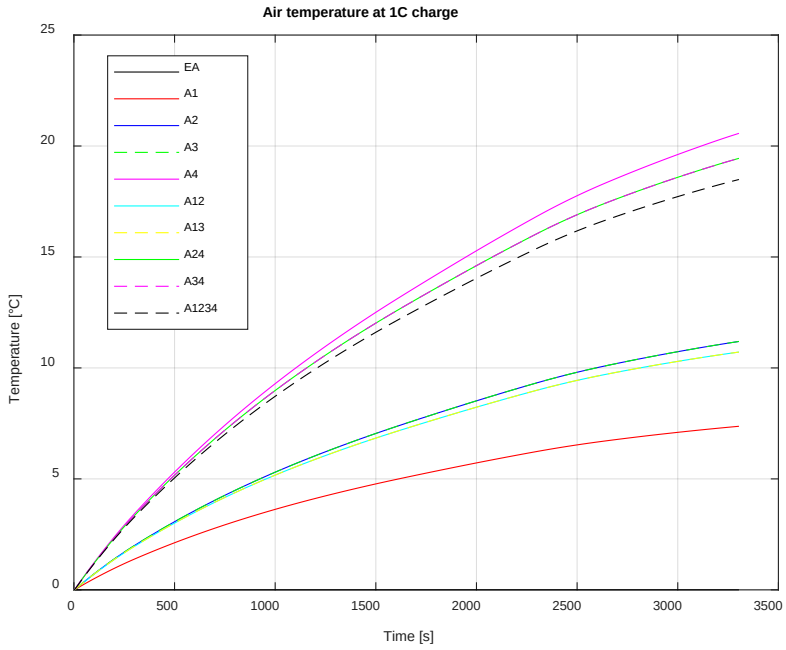

Figure 22: Air temperatures during 1C-charging

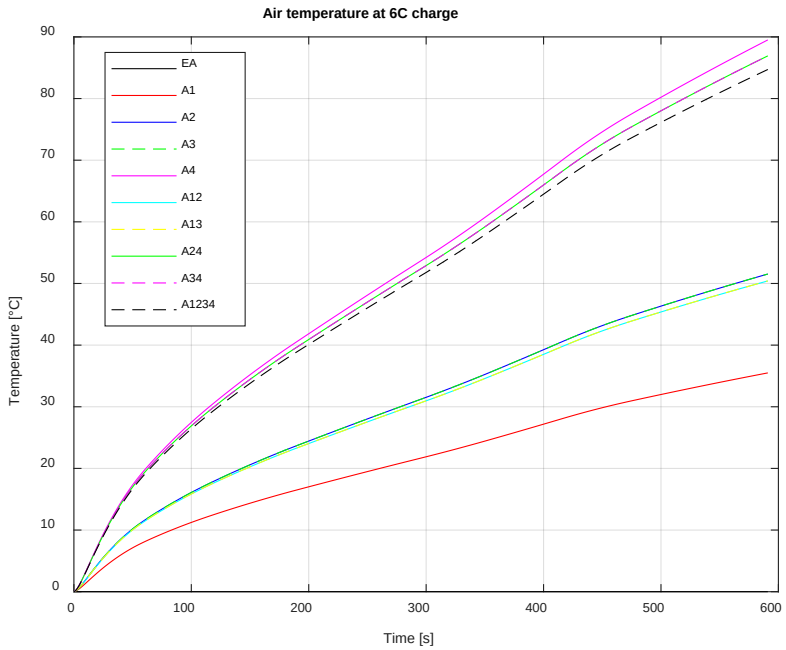

Figure 23: Air temperatures during 6C-ultra-fast-charging

Fig. 22-23 display the results of the temperature evolution of the air inside the module configuration for both studied charging rates. It is noteworthy that the air temperature increases much faster for the 6C case, showing dangerous high temperature gradients within a very short time. Also, the temperature within the module is non-uniform, as there is a difference of about 55ºC between the coldest and hottest air nodes. Even for the 1C normal charge rate, this difference is about 15ºC. This is negative for the battery operation, as it is important that the temperature distribution within the module is uniform to achieve optimum performance[53].

This explains why air-cooling systems are giving way to batteries' thermal management systems based on other types of fluids, such as liquid or immersion cooling. These use dielectric liquids, characterized by thermal properties that are much more efficient than those for indirect liquid cooling or air

7. Conclusions

In this work, a lumped thermal model for the characterization of lithium-ion batteries has been developed, validated with some experimental measurements and applied to a module at normal and ultra-fast charging operation conditions. The development of lumped thermal models is fundamental not only to have a comprehension of the thermal behavior of the battery under different constraints and input conditions, but also to reduce calculations time with respect to the use of physically based models. In addition, lumped models do not require any deep knowledge of all the phenomena happening inside the battery (electrochemistry, mass transport, diffusion), while still allowing for a good description of the cell and module behavior. The kind of model developed within this work can be easily integrated in the strategies of control and management of temperature in a battery management system [54]. It would help estimate in real-time the thermal behavior of a vehicle battery pack to avoid reaching dangerous levels of temperature, that may compromise both the safety of the operations and the optimal performance of the battery pack.

The model presented in this work has been used to conduct an analysis of a stand-alone cell and a battery module configuration in ultra-fast charging conditions. The potential to easily model module and pack configurations allows the user to have an initial understanding of the thermal behavior of a solution for electrified vehicles. The methodology proposed, comprising an experimental measurement campaign, the characterization of the electrical and thermal parameters and validation of the model can be easily replicated for any other cylindrical cell, giving the model almost limitless possibilities to be used.

Acknowledgments

This work was supported by Generalitat Valenciana within the framework of the PROMETEO project "Contribution to the decarbonization of transport by optimizing the

thermal management of vehicle batteries electrified" with reference number PROMETEO/2020/042.

References

[1] X. Li *et al.*, “Numerical study on the effects of intake charge on oxy-fuel combustion in a dual-injection spark ignition engine at economical oxygen-fuel ratios,” *Int. J. Engine Res.*, 2021, doi: 10.1177/14680874211022292.

[2] W. Vera-Tudela, C. Barro, and K. Boulouchos, “Investigations on spark pre-chamber ignition and subsequent turbulent jet main chamber ignition in a novel optically accessible test rig,” *Int. J. Engine Res.*, pp. 1–13, 2021, doi: 10.1177/14680874211019849.

[3] S. Tavakoli, K. M. Bagherabadi, J. Schramm, and E. Pedersen, “Fuel consumption and emission reduction of marine lean-burn gas engine employing a hybrid propulsion concept,” *Int. J. Engine Res.*, vol. 0, no. 0, p. 14680874211016398, doi: 10.1177/14680874211016398.

[4] M. C. Joshi, D. Gosala, G. M. Shaver, J. McCarthy, and L. Farrell, “Exhaust valve profile modulation for improved diesel engine curb idle aftertreatment thermal management,” *Int. J. Engine Res.*, 2021, doi: 10.1177/1468087420969101.

[5] H. Liu, Z. Wei, W. He, and J. Zhao, “Thermal issues about Li-ion batteries and recent progress in battery thermal management systems: A review,” *Energy Convers. Manag.*, vol. 150, no. May, pp. 304–330, 2017, doi: 10.1016/j.enconman.2017.08.016.

[6] N. Sato, “Thermal behavior analysis of lithium-ion batteries for electric and hybrid vehicles,” *J. Power Sources*, vol. 99, no. 1–2, pp. 70–77, 2001, doi: 10.1016/S0378-7753(01)00478-5.

[7] L. H. Saw, Y. Ye, and A. A. O. Tay, “Integration issues of lithium-ion battery into electric vehicles battery pack,” *J. Clean. Prod.*, vol. 113, pp. 1032–1045, 2016, doi: 10.1016/j.jclepro.2015.11.011.

[8] H. Lundgren *et al.*, “Thermal Management of Large-Format Prismatic Lithium-Ion Battery in PHEV Application,” *J. Electrochem. Soc.*, vol. 163, no. 2, pp. A309–A317, 2016, doi: 10.1149/2.09411602jes.

[9] H. Rahimi-Eichi, U. Ojha, F. Baronti, and M. Y. Chow, “Battery management system: An overview of its application in the smart grid and electric vehicles,” *IEEE Ind. Electron. Mag.*, vol. 7, no. 2, pp. 4–16, 2013, doi: 10.1109/MIE.2013.2250351.

[10] M. Nizam, H. Maghfiroh, R. A. Rosadi, and K. D. U. Kusumaputri, “Battery management system design (BMS) for lithium ion batteries,” *AIP Conf. Proc.*, vol. 2217, no. April, 2020, doi: 10.1063/5.0000649.

[11] R. Rizk, H. Louahlia, H. Gualous, and P. Schaetzel, “Experimental analysis and transient thermal modelling of a high capacity prismatic lithium-ion battery,” *Int. Commun. Heat Mass Transf.*, vol. 94, pp. 115–125, 2018, doi: 10.1016/j.icheatmasstransfer.2018.03.018.

[12] D. Li and L. Yang, “Identification of spatial temperature gradient in large format lithium battery using a multilayer thermal model,” *Int. J. Energy Res.*, vol. 44, no. 1, pp. 282–297, 2020, doi: 10.1002/er.4914.

[13] C. Forgez, D. Vinh Do, G. Friedrich, M. Morcrette, and C. Delacourt, “Thermal modeling of a cylindrical LiFePO4/graphite lithium-ion battery,” *J. Power Sources*, vol. 195, no. 9, pp. 2961–2968, 2010, doi: 10.1016/j.jpowsour.2009.10.105.

[14] M. Akbarzadeh *et al.*, “Thermal modeling of a high-energy prismatic lithium-ion battery cell and module based on a new thermal characterization methodology,” *J. Energy Storage*, vol. 32, no. April, p. 101707, 2020, doi: 10.1016/j.est.2020.101707.

[15] Y. wei Pan *et al.*, “A computational multi-node electro-thermal model for large prismatic lithium-ion batteries,” *J. Power Sources*, vol. 459, no. November 2019, p. 228070, 2020, doi: 10.1016/j.jpowsour.2020.228070.

[16] Damay, Nicolas, et al. "Thermal modeling of large prismatic LiFePO4/graphite battery. Coupled thermal and heat generation models for characterization and simulation." *Journal of Power Sources* 283 (2015): 37-45.

[17] K. Makinejad *et al.*, “A lumped Electro-thermal model for Li-Ion cells in electric vehicle application,” *World Electr. Veh. J.*, vol. 7, no. 1, pp. 1–13, 2015, doi: 10.3390/wevj7010001.

[18] X. Lin *et al.*, “A lumped-parameter electro-thermal model for cylindrical batteries,” *J. Power Sources*, vol. 257, pp. 12–20, 2014, doi: 10.1016/j.jpowsour.2014.01.097.

[19] M. A. Perez Estevez, S. Calligaro, O. Bottesi, C. Caligiuri, and M. Renzi, “An electro-thermal model and its electrical parameters estimation procedure in a lithium-ion battery cell,” *Energy*, vol. 234, p. 121296, 2021, doi: 10.1016/j.energy.2021.121296.

[20] Flores, Mirna Maricela Martínez, et al. "Implementation of control algorithms in a climatic chamber." *2016 International Conference on Mechatronics, Electronics and Automotive Engineering (ICMEAE)*. IEEE, 2016.

[21] ARBIN, “ARBIN INSTRUMENTS Laboratory Battery Testing System For Cell Applications Product Description Experts in Test Instrumentation,” vol. 1, no. 979, pp. 1–7.

[22] Agilent, “Agilent 34970A Data Acquisition / Switch Unit Family,” *Documentation*, vol. 90012, no. 34970, pp. 1–28, 2012.

[23] Datasheet NX, “Ref : ACL9074 LiFePO4 BATTERY 26650,” pp. 4–5, 2020.

[24] Plett, Gregory L. *Battery management systems, Volume I: Battery modeling*. Artech House, 2015.

[25] M. Petzl and M. A. Danzer, “Advancements in OCV measurement and analysis for lithium-ion batteries,” *IEEE Trans. Energy Convers.*, vol. 28, no. 3, pp. 675–681, 2013, doi: 10.1109/TEC.2013.2259490.

[26] L. Ren, G. Zhu, J. V. Wang, B. Luo, and J. Kang, “Comparison of robustness of

different state of charge estimation algorithms," *J. Power Sources*, vol. 478, no. July, p. 228767, 2020, doi: 10.1016/j.jpowsour.2020.228767.

[27] L. Lu, X. Han, J. Li, J. Hua, and M. Ouyang, "A review on the key issues for lithium-ion battery management in electric vehicles," *J. Power Sources*, vol. 226, no. March, pp. 272–288, 2013, doi: 10.1016/j.jpowsour.2012.10.060.

[28] K. Wang *et al.*, "Internal resistance and heat generation of soft package Li4Ti5O12 battery during charge and discharge," *Energy*, vol. 149, pp. 364–374, 2018, doi: 10.1016/j.energy.2018.02.052.

[29] Liaw, Bor Yann, et al. "Modeling of lithium ion cells—A simple equivalent-circuit model approach." *Solid state ionics* 175.1-4 (2004): 835-839.

[30] G. Liu, M. Ouyang, L. Lu, J. Li, and X. Han, "Analysis of the heat generation of lithium-ion battery during charging and discharging considering different influencing factors," *J. Therm. Anal. Calorim.*, vol. 116, no. 2, pp. 1001–1010, 2014, doi: 10.1007/s10973-013-3599-9.

[31] A. Nazari and S. Farhad, "Heat generation in lithium-ion batteries with different nominal capacities and chemistries," *Appl. Therm. Eng.*, vol. 125, pp. 1501–1517, 2017, doi: 10.1016/j.applthermaleng.2017.07.126.

[32] Torregrosa, Antonio Jose, et al. "Assessment of the improvement of internal combustion engines cooling system using nanofluids and nanoencapsulated phase change materials." *International Journal of Engine Research* 22.6 (2021): 1939-1957.

[33] He, Hongwen, Rui Xiong, and Jinxin Fan. "Evaluation of lithium-ion battery equivalent circuit models for state of charge estimation by an experimental approach." *energies* 4.4 (2011): 582-598.

[34] S. S. Zhang, K. Xu, and T. R. Jow, "The low temperature performance of Li-ion batteries," *J. Power Sources*, vol. 115, no. 1, pp. 137–140, 2003, doi: 10.1016/S0378-7753(02)00618-3.

[35] L. Liao *et al.*, "Effects of temperature on charge/discharge behaviors of LiFePO 4 cathode for Li-ion batteries," *Electrochim. Acta*, vol. 60, no. February, pp. 269–273, 2012, doi: 10.1016/j.electacta.2011.11.041.

[36] X. Wang, X. Wei, and H. Dai, "Estimation of state of health of lithium-ion batteries based on charge transfer resistance considering different temperature and state of charge," *J. Energy Storage*, vol. 21, no. January, pp. 618–631, 2019, doi: 10.1016/j.est.2018.11.020.

[37] T. R. Jow, S. A. Delp, J. L. Allen, J.-P. Jones, and M. C. Smart, " Factors Limiting Li + Charge Transfer Kinetics in Li-Ion Batteries ," *J. Electrochem. Soc.*, vol. 165, no. 2, pp. A361–A367, 2018, doi: 10.1149/2.1221802jes.

[38] N. E. Galushkin, N. N. Yazvinskaya, and D. N. Galushkin, "Generalized Analytical Model for Capacity Evaluation of Automotive-Grade Lithium Batteries," *J. Electrochem. Soc.*, vol. 162, no. 3, pp. A308–A314, 2015, doi: 10.1149/2.0311503jes.

[39] N. Omar, P. Van den Bossche, T. Coosemans, and J. Van Mierlo, "Peukert revisited-critical appraisal and need for modification for lithium-ion batteries,"

Energies, vol. 6, no. 11, pp. 5625–5641, 2013, doi: 10.3390/en6115625.

[40] D. I. Stroe, M. Swierczynski, A. I. Stroe, and S. K. Kær, "Generalized characterization methodology for performance modelling of lithium-ion batteries," *Batteries*, vol. 2, no. 4, 2016, doi: 10.3390/batteries2040037.

[41] T. Inl, "Battery Test Manual for Plug-In Hybrid Electric Vehicles," *Contract*, vol. 158, no. March, pp. 1720–1723, 2010.

[42] A. I. Pózna, K. M. Hangos, and A. Magyar, "Temperature dependent parameter estimation of electrical vehicle batteries," *Energies*, vol. 12, no. 19, pp. 1–17, 2019, doi: 10.3390/en12193755.

[43] Mathewson, Scott. *Experimental measurements of LiFePO4 battery thermal characteristics*. MS thesis. University of Waterloo, 2014.

[44] Lin, Cheng, et al. "Research on thermo-physical properties identification and thermal analysis of EV Li-ion battery." *2009 IEEE Vehicle Power and Propulsion Conference*. IEEE, 2009.

[45] A. S. F. P., DeWitt, D. P., Bergman, T. L., & Lavine, *Fundamentals of heat and mass transfer (Vol. 6)*. 1996.

[46] S. Ahmed *et al.*, "Enabling fast charging – A battery technology gap assessment," *J. Power Sources*, vol. 367, pp. 250–262, 2017, doi: 10.1016/j.jpowsour.2017.06.055.

[47] T. R. Tanim *et al.*, "Heterogeneous Behavior of Lithium Plating during Extreme Fast Charging," *Cell Reports Phys. Sci.*, vol. 1, no. 7, 2020, doi: 10.1016/j.xcrp.2020.100114.

[48] X. G. Yang, G. Zhang, S. Ge, and C. Y. Wang, "Fast charging of lithium-ion batteries at all temperatures," *Proc. Natl. Acad. Sci. U. S. A.*, vol. 115, no. 28, pp. 7266–7271, 2018, doi: 10.1073/pnas.1807115115.

[49] A. Tomaszewska *et al.*, "Lithium-ion battery fast charging: A review," *eTransportation*, vol. 1, no. August, p. 100011, 2019, doi: 10.1016/j.etran.2019.100011.

[50] J. B. Habedank, J. Kriegler, and M. F. Zaeh, "Enhanced Fast Charging and Reduced Lithium-Plating by Laser-Structured Anodes for Lithium-Ion Batteries," *J. Electrochem. Soc.*, vol. 166, no. 16, pp. A3940–A3949, 2019, doi: 10.1149/2.1241915jes.

[51] K. C. Chiu, C. H. Lin, S. F. Yeh, Y. H. Lin, C. S. Huang, and K. C. Chen, "Cycle life analysis of series connected lithium-ion batteries with temperature difference," *J. Power Sources*, vol. 263, pp. 75–84, 2014, doi: 10.1016/j.jpowsour.2014.04.034.

[52] P. Dubey, G. Pulugundla, and A. K. Srouji, "Direct comparison of immersion and cold-plate based cooling for automotive li-ion battery modules," *Energies*, vol. 14, no. 5, 2021, doi: 10.3390/en14051259.

[53] S. Shahid and M. Agelin-Chaab, "Development and analysis of a technique to improve air-cooling and temperature uniformity in a battery pack for cylindrical batteries," *Therm. Sci. Eng. Prog.*, vol. 5, no. November 2017, pp. 351–363, 2018,

doi: 10.1016/j.tsep.2018.01.003.

[54] J. Hou, M. Yang, D. Wang, and J. Zhang, “Fundamentals and Challenges of Lithium Ion Batteries at Temperatures between −40 and 60 °C,” *Adv. Energy Mater.*, vol. 10, no. 18, pp. 1–23, 2020, doi: 10.1002/aenm.201904152.

[55] T. M. Bandhauer, S. Garimella, and T. F. Fuller, “A Critical Review of Thermal Issues in Lithium-Ion Batteries,” *J. Electrochem. Soc.*, vol. 158, no. 3, p. R1, 2011, doi: 10.1149/1.3515880.

[56] FLIR SYSTEMS, "ThermaCAM™ P60, The professional thermographer's choice", 2002